Author/s:
Girotra, M;Srivastava, S;Kulkarni, A;Barbora, A;Bobra, K;Ghosal, D;Devan, P;Aher, A;Jain, A;Panda, D;Ray, K

Title:
The C-terminal tails of heterotrimeric kinesin-2 motor subunits directly bind to α-tubulin1: Possible implications for cilia-specific tubulin entry

Date:
2017-02-01

Citation:
Girotra, M., Srivastava, S., Kulkarni, A., Barbora, A., Bobra, K., Ghosal, D., Devan, P., Aher, A., Jain, A., Panda, D. & Ray, K. (2017). The C-terminal tails of heterotrimeric kinesin-2 motor subunits directly bind to α-tubulin1: Possible implications for cilia-specific tubulin entry. Traffic, 18 (2), pp.123-133. https://doi.org/10.1111/tra.12461.

Original Research Article
TRA.12461
doi: 10.1111/TRA.12461
Society number TRA-15-0375
NIH funded NO
Manuscript received 1 May 2015
Revised and accepted 6 December 2016
Sent to press 6 December 2016
Color figures: Figures 1, 2, 3, 4, 5, 6
Supplemental figures (legends only to be included in typeset manuscript): 4 tables, 4 videos, 6 figures
Synopsis included YES
Abstract figure included YES
Editorial process file included NO

The C-terminal tails of heterotrimeric kinesin-2 motor subunits directly bind to α-tubulin1: possible implications for cilia-specific tubulin entry

Mukul Girotra[1a§], Shalini Srivastava[2§], Anuttama Kulkarni[1b§], Ayan Barbora[1], Kratika Bobra[1], Debnath Ghosal[1c], Pavithra Devan[1], Amol Aher[1d], Akanksha Jain[1e], Dulal Panda[2], Krishanu Ray[1]*

[1]Tata Institute of Fundamental Research, Homi Bhabha Road, Mumbai 400005, [2]Department of Biosciences and Biotechnology, Indian Institute of Technology-Bombay, Powai, Mumbai 400076, India

Corresponding Author: Department of Biological Sciences, Tata Institute of Fundamental Research, Homi Bhabha Road, Mumbai 400005. E-mail: krishanu@tifr.res.in, Telephone: +912222782730, Fax: +912222804610.
ORCiD ID. orcid.org/0000-0001-6406-3199

Running Title: Kinesin-2 tails bind α-tubulin1

Keywords: Kinesin-like-protein 64D, Kinesin-like-protein 68D, Kif3A, Kif3B, Cilia, Antenna, *Drosophila*, Mouse.

Present Address:
a) Ludwig Institute for Cancer Research (LICR), University of Lausanne (UNIL), Switzerland.
b) Department of Life Sciences, Sophia College, Mumbai, India.
c) Division of Biology, California Institute of Technology, Pasadena, CA, USA.
d) Cell Biology, Faculty of Science, Utrecht University, Netherlands.
e) Max Planck Institute of Molecular Cell Biology and Genetics, Dresden, Germany.

§ - authors made an equal contribution to the manuscript.

eTOC Synopsis

Tubulin entry into the cilia and flagella is essential for their growth. The article by Girotra et al., suggests that the tail domains of heterotrimeric Kinesin-2 motor subunits can selectively bind certain α-tubulin1 isotypes and regulate the entry of tubulin into cilia. The conjecture is supported by extensive binding studies *in vitro* and tissue-cultured cells using recombinant tail fragments of both *Drosophila* and mouse orthologues, as well as genetic analysis in *Drosophila.*

Abstract

The assembly of microtubule-based cytoskeleton propels the cilia and flagella growth. Previous studies have indicated that the kinesin-2 family motors transport tubulin into the cilia through intraflagellar transport. Here, we report a direct interaction between the C-terminal tail fragments of heterotrimeric kinesin-2 and α-tubulin1 isoforms in vitro. Blot overlay screen, affinity purification from tissue extracts, cosedimentation with subtilisin-treated microtubule and LC-ESI-MS/MS characterization of the tail-fragment-associated tubulin identified an association between the tail domains and α-tubulin1A/D isotype. The interaction was confirmed by FRET assay in tissue cultured cells. The overexpression of the recombinant tails in NIH3T3 cells affected the primary cilia growth which was rescued by coexpression of a α-tubulin-1 transgene. Furthermore, FRAP analysis in the olfactory cilia of *Drosophila* indicated that tubulin is transported in a non-particulate form requiring kinesin-2. These results provide additional new insight into the mechanisms underlying selective tubulin isoform enrichment in the cilia.

Introduction

Primary cilia and flagella are the most widely expressed cellular appendages that act as a signaling center of a eukaryotic cell [1]. Specialized microtubule-based cytoskeleton, called axoneme, supports the cilia and flagella [2]. The sensory cilia, further diversified for the reception of various kind of stimuli, mostly contains a bipartite structure [3]. The bipartite sensory cilium, such as the olfactory cilia, is supported by two distinct types of microtubule cytoskeleton – the 9+0 doublet microtubule-bearing axoneme at the proximal end and the singlet microtubule bearing outer segment [4, 5]. Distinct tubulin isotypes are shown to localize in the flagella [6] and at different parts of a sensory cilium[7]. Microtubule grows at the plus-end. Amongst many other components, it depends on the local availability of dissociated tubulin [8]. The tubulin transport plays a critical role defining the rate of microtubule growth inside the narrow appendages, such as the cilia and flagella. Therefore, it is evident that an active and selective tubulin transport assembles the cilia and flagella.

Kinesin-2 represents two conserved subfamilies of heterotrimeric and homodimeric motors found in organisms ranging from *Chlamydomonas* to humans [9]. It is essential for the ciliary and flagellar assembly [10]. The anterograde transport into the flagella involving the intraflagellar transport (IFT) complex requires kinesin-2 [11, 12]. Also, mutations in the kinesin-2 motor subunit genes, as well as the IFT subunits disrupts the cilia and flagella assembly [4, 13-16]. In *Chlamydomonas* flagella, tubulin is transported by a combination of IFT and free diffusion [17]. In the sensory cilia of *C. elegans*, tubulin moves in a particulate form requiring the cooperative action of heterotrimeric and homodimeric kinesin-2 motors [18]. Also, tubulin is shown to bind to the IFT 74/81 complex through cooperative interaction [19]. Altogether these results indicated that tubulin could be transported into the cilia/flagella through a combination of active transport and diffusion. These reports, however, do not explain how particular tubulin isotypes are enriched into the cilia and flagella.

The C-terminal tail domains of kinesin-1 and 14 were reported to bind microtubule directly [20, 21]. These interactions are suggested to regulate the motor function and microtubule bundling in vivo. Interestingly, a significant amount of heterotrimeric kinesin-2 were also found to associate with microtubule in an ATP-independent manner [22]. Hence, it raised a possibility that kinesin-2 could bind microtubule through a second site.

The molecular basis of cargo-motor interactions involving kinesin-2 is still poorly defined. The motor binds to cargoes through its stalk-tail domain and a variety of different adaptors [23-27]. Besides binding to

choline acetyltransferase [28] and Syne-1 [29] little is known about the kinesin-2 tail-interacting proteome. Here, we provide evidence to suggest that the motor subunits of heterotrimeric kinesin-2 could directly bind to dissociated tubulin in vitro through the respective C-terminal tail domains. LC- ESI-MS/MS analysis of the tubulin pool, co-purified with kinesin-2 tail fragments, indicated a preferential association with the α-Tubulin1 isotype. Moreover, overexpression of recombinant kinesin-2 tails disrupted primary cilia assembly in NIH3T3 cells. The phenotype was reversed due to coexpression of a α-Tubulin1 isoform. Moreover, tubulin was found to be transported in a non-particulate form into the outer segment of the cilia on *Drosophila* olfactory neurons. Altogether, these results suggest that both the kinesin-2 tails are capable of binding to free tubulin dimer, which may facilitate selective tubulin entry into the sensory cilia during growth phases.

Results:

Recombinant kinesin-2 tail fragments associated with tubulin in cellular extracts

Affinity purification from the *Drosophila* head extracts expressing the poly-histidine tagged, full-length KLP64D pulled down tubulin along with other kinesin-2 subunits (Figure 1B). Tubulin was also immunoprecipitated from mouse brain extracts using anti-Kif3A (Figure S1) in ATP-devoid conditions. Together, these two results indicated that heterotrimeric kinesin-2 could bind to tubulin in dissociated form. There are two possible sites for tubulin binding in a motor complex – the head and the tail domains. A blot overlay assay using GST-KLP64DT (KLP64D Tail) and GST-KLP68DT (KLP68D Tail), respectively, highlighted multiple bands in both the *Drosophila* and mouse brain extracts (Figure 1B, Figure S1). Amongst them, the 52kDa band (arrow, Figure 1B) was the most prominent one. Subsequent affinity copurifications of tubulin with the GST-KLP64DT and GST-KLP68DT from tissue extracts (Figure 1D) and co-sedimentation of the tail fragments with microtubule (Figure 1E and F), further indicated a possible direct interaction between tubulin and the tail domains.

Also, to demonstrate that the tail domains of heterotrimeric kinesin-2 could bind to tubulin, we expressed either KLP64D-Tev-His or tail-less KLP64DΔT-Tev-His along with KLP68DΔT-YFP in *Drosophila* and affinity purified the recombinant motors using Ni-NTA in presence and absence of 20 μM colchicine. The presence of colchicine visibly reduced the level of tubulin pulled down with KLP64D-Tev-His (Figure 1G), and disrupted tubulin copurification with the KLP64DΔT-Tev-His, indicating that the tail domains of heterotrimeric kinesin-2 could bind to tubulin under physiological conditions.

Previous in vitro studies reported that the C-terminal tail fragments of kinesin-1 and 14 could bind to microtubule with a submicromolar affinity [30, 31]. We found that the GST-Kif3A tail could cosediment with microtubule filaments with an affinity of 3.6+1.8 μM (Figure S1), indicating that kinesin-2 tails have a comparatively much weaker affinity to the microtubule. Kinesin-2 tails contain several conserved, positively charged islands flanked by proline, and they are predicted to be unfolded (Supplementary Data). Similar amino acid organizations are found in tubulin binding regions of tau, MAP2C, kinesin-1 [30] and kinesin-14 [20] tails.

C-terminal region of α-tubulin is required for microtubule decoration by the kinesin-2 tail fragments

The specificity of tail-tubulin interaction was further verified using microtubule decoration assay on coverslips (Figure 2A). The recombinant GST-KLP64DT and GST-KLP68DT tail polypeptides (concentrations, 1 μM) decorated taxol-stabilized microtubule in a flow cell (Figure 2A). We noticed that the GST-tail labeling was patchy and excluded the antibody stained regions (Inset, Figure 2A). Also, preincubation with the α-tubulin antibody (12G10, dil. 1:1000), blocked the tail decoration of microtubule (Figure 2B), indicating that the tails bind on the solvent-exposed sites of tubulin subunits on a microtubule. The kinesin-1 tail competes with the tau binding sites on microtubule and interacts with the β-tubulin subunit at a site distinct from that of the motor domain [21], whereas the kinesin-14 tail binds to both the α- and β-tubulin [32].

Although both α- and β-tubulin are highly homologous, the short (10-15 aa), C-terminal E-hook sequences provide distinct subunit and isoform identity to tubulins. Subtilisin is known to clip the C-terminal region of β-tubulin subunits preferentially at specified conditions [33]. Using these conditions, we generated microtubule preparations devoid of C-terminal regions of either the β-subunit ($\alpha\beta^s$) or both the β- and α-subunits ($\alpha^s\beta^s$, Figure 2C). The affinity purified 6xHis-sYFP-KLP64DT, as well as 6xHis-sYFP-KLP68DT, cosedimented with the $\alpha\beta^s$ microtubule at a level visually comparable to that of the control (Figure 2D). The levels of tails cosedimented with the $\alpha^s\beta^s$ microtubule were, however, visibly reduced (Figure 2D). The C-terminal regions are essential for binding with both kinesin-1 [30] and kinesin-14 [31] tails. For kinesin-14 tail, which binds to four independent sites on tubulin subunits, including the E-hooks of α- and β-subunits [32, 34], the interactions with the $\alpha\beta^s$ and $\alpha^s\beta^s$ microtubule are only partly reduced [32]. In contrast, the interaction between the kinesin-1 tail and $\alpha^s\beta^s$ was reported to be reduced earlier [30]. Thus, we found a distinctly different pattern of interactions between the $\alpha\beta^s$ and $\alpha^s\beta^s$ microtubule and kinesin-2 tail fragments. It indicated that the tubulin C-terminus, in particular, the E-hook region of α-tubulin is essential for the binding.

Kinesin-2 tail fragments selectively associate with tubulin in the brain and kidney extracts

Next, to test the interactions between the kinesin-2 tails and cellular microtubule, we expressed sYFP-KLP64DT and sYFP-KLP68DT in NIH3T3 cells (Figure 3A). Consistent with a previous report [35], the sYFP-tagged tail fragments colocalized with the endoplasmic reticulum (Figure S2). There was no detectable decoration of the cellular microtubule (inset, Figure 3A). It was further confirmed by loading HeLa cells with purified GST-KLP64DT and GST-KLP68DT using the glass bead loading technique. Once again, the majority of GST-KLP64DT and GST-KLP68DT were localized in the cytoplasm (Figure 3B). A similar overexpression of kinesin-1 tail fragment decorated the cellular microtubule in specific cell types [36-38]. Thus, our observation raised an intriguing possibility that the kinesin-2 tail-tubulin interaction could be limited to certain tissue or subcellular domain-specific forms of α-tubulin. Therefore, we estimated tubulin pull down from different tissue preparations using affinity chromatography. The recombinant kinesin-2 tails pulled down tubulin from the mouse brain extracts in proportionately higher levels, and GST-KLP68DT also pulled down a relatively higher amount from the kidney extract (Figure 3C). In comparison, a majority of the tubulin from sciatic nerve (SN), liver (L) and muscle (M), failed to bind the GST-tail fragments (Figure 3C), indicating a preferential association between the tails and brain tubulin.

The neuronal microtubule is extensively modified. It contains high levels of acetylated, detyrosinated and Δ2 α-tubulin [39], as well as polyaminated β-tubulin [40]. The C-terminal E-hook region of tubulin subunits is also extensively glutamylated and glycylated [39]. These alterations increase local negative charge density that makes the microtubule stable and insoluble. Our data suggested that kinesin-2 tails are likely to bind soluble tubulin through a combination of charge based and non-ionic interactions. In addition, a significant amount of acetylated α-tubulin was pulled down by the recombinant tails from the goat brain tubulin preparations (Figure S3), indicating that tubulin acetylation may not alter the binding to the recombinant tails. Therefore, we reasoned that post-translational modifications are unlikely to reduce the pull-down efficiency selectively from the soluble extract of the sciatic nerve. The kidney, on the other hand, contains a large number of long ciliated cells, and kinesin-2 is known to transport distinct tubulin isotypes into the cilia through IFT [18]. We found that the kidney tubulin had a relatively higher affinity to the KLP68DT. Hence, we conjectured that kinesin-2 tails could selectively bind to the α-tubulin isotypes present in the neuronal cell body and dendrites of the brain tissue, as well as in the kidney.

Both the kinesin-1 and 14 tails bind to β-tubulin subunit and stabilizes microtubule assembly in vitro [20, 30]. A quantitative co-sedimentation analysis showed that the interactions between kinesin-2 tails and tubulin did not cross-link (Figure 3D) or stabilize (Figure 3E) the microtubule. The recombinant tails also pulled down dissociated tubulin from GTP depleted preparations (Figure S3). Thus, it further suggested that kinesin-2 tails could directly bind to tubulin dimers in solution. Together with the above

results it also suggested that kinesin-2 tails might help the motor transport soluble tubulin in brain and kidney cells.

Kinesin-2 tails preferentially bind to the α-tubulin1 isoforms in vitro

α-Tubulin 1, 2 and 4 isotypes are expressed in mammalian brain [41, 42], and mouse brain predominantly contains α1A, α1B and α1C isoforms [43]. To identify the candidate tubulin isoform that binds to kinesin-2 tails, we analyzed the composition of tubulin, copurified with the recombinant tail fragments using LC-ESI-MS/MS (Figure 4A-B). We reasoned that if the tails indeed bind to particular isotypes, then those will be the dominant component in the pulled down content. Therefore, we set a relatively high cut-off for the M/Z counts and selected the most dominant entities for each M/Z value zone.

As expected, the analysis of input tubulin did not identify any dominant α- or β-tubulin isoforms. The LC peaks were highly degenerate, and the M/Z counts were also significantly low as compared to the tubulin samples collected through the copurification. In contrast, peptides obtained from tubulin copurified with kinesin-2 tails were mainly eluted in few overlapping LC fractions (Figure 4B). Furthermore, the M/Z counts for these peptides were significantly higher, with highly correlated occurrence patterns. A database search with the M/Z values of the pulled down peptides matched to the α-tubulin1A sequences with the maximum confidence scores (Table S1 and S2). Furthermore, two of the peptides pulled down by the KLP68D tail also matched to α-tubulin1D, although it did not rule out the possibility of α-Tubulin1A-C binding to KLP68DT. The assignments were made on the high probability score. In contrast, immunostaining the western blots of the kinesin-2 tail pull-down products with the β-tubulin isotype-specific antibodies identified all five (βI-V) isoforms in proportions similar to the input (Figure S4). These data suggested that recombinant kinesin-2 tails bind to the α-tubulin1 isotype with a relatively higher affinity. Aspergillus kinesin-3 (UncA) is also shown to bind α-tubulin subunit in vivo through a bimolecular fluorescence assay [44]. However, it is unclear whether it also recognized a particular isotype.

To validate the kinesin-2 tail-tubulin interaction in the cellular environment, we used the Forster's Resonance Energy Transfer (FRET) assay to estimate binding between a recombinant tubulin isoform and kinesin-2 tail fragments in tissue-cultured cells. A similar assay was utilized to test the interaction between kinesin-1 and microtubule earlier [45]. *Drosophila* Tubulin84B, primarily enriched in the outer segments of the sensory cilia [4, 46], is homologous to the α-tubulin1C/D and 3A (Supplemental Data IV). An N-terminal fusion construct of this protein with mTurquoise (TQ, Ex 434 nm, Em 473 nm) was expressed in NIH3T3 cells along with yellow fluorescent protein (sYFP, Ex 514 nm and Em 540 nm) conjugated kinesin-2 tails, sYFP-KLP64DT and sYFP-KLP68DT, respectively (Figure 4D). The majority of TQ-Tub84B did not incorporate in the cellular microtubule. Also, the FRET emission from the sYFP, conjugated to kinesin-2 tails, were mostly distributed in the cytoplasm (Figure 4D), indicating that the tails are likely to bind unpolymerized tubulin within a cell.

FRET analysis also revealed that recombinant TQ-Tub84B could associate with both KLP64DT and KLP68DT, respectively (Figure 4D). The FRET efficiency, estimated using the sensitized-FRET protocol [47], suggested that the interaction between TQ-Tub84B and sYFP-KLP64DT was high and comparable to the values obtained from the TQ-6aa-sYFP conjoined protein (Table S3). The interaction with sYFP-KLP68DT was comparatively less efficient than the sYFP-KLP64DT. The sYFP-KLP68DT could bind to a wider number of proteins in the cell, and this could affect the interaction with the recombinant tubulin. Alternatively, the results may indicate that the interaction is indeed the strongest with KLP64DT.

Although the recombinant tails pulled down α-Tubulin1 isotypes from the brain preparation, they failed to decorate stable microtubule in HeLa cells which predominantly contains α-Tubulin1B isoform [43]. This result was intriguing because the pull-down analysis suggested that the tails bind to dissociated tubulin, and we found that the principal amount of FRET between the recombinant TUB84B and tail fragments occurred in the cytoplasm of live NIHT3T cells. We reasoned that the paraformaldehyde fixation protocol used for the earlier experiments

would mostly retain stable microtubules and a significant fraction of the recombinant tail-tubulin complex would be washed off during fixation.

Kinesin-2 tails are essential for primary cilia growth in tissue-cultured cells

Primary cilia are unique cellular appendages entirely supported by a microtubule-based cytoskeleton and IFT by heterotrimeric kinesin-2. Although it is unclear how the IFT complex associates with the kinesin-2, the IFT20 subunit is shown to bind to the stalk domain of KIF3B (Kinesin-2β subunit) in vitro [26]. Therefore, we decided to test the effect of the tail overexpression on the cilia growth in NIH3T3 cells. It was not expected to block IFT-mediated transport into the cilia. Overexpression of sYFP-KLP64DT and sYFP-KLP68DT, respectively, reduced cilia growth after serum starvation in NIH3T3 cells significantly (Figure 5A and C). The tail overexpression, however, did not disrupt the basal body and cellular microtubule, suggesting that the intervention selectively targeted cilia growth.

Cilia loss may occur due to general sequestration of ciliary proteins transported by kinesin-2 in the cytosol. It could be reverted by saturating the cytosol with a proportional amount of a 'tail-interacting' protein. Consistent with this hypothesis we found that the expression of TQ-Tub84B along with the sYFP-tails rescued the defects (Figure 5B and C), whereas that of the Arl13b, a membrane-associated protein selectively enriched in the cilia [48], did not alter the defect (Figure 5D and E). Both IFT-dependent [49, 50] and independent [51] processes are implicated in the transport of the transmembrane proteins into the cilia. The small GTPase, Rab23, plays an important rile in these transports [48]. Therefore, it is unlikely that Arl13b could directly interact with kinesin-2. Hence, these results further indicated that kinesin-2 tails directly bind to tubulin in a cellular environment. It also indicated that tubulin could compete with other essential cargoes for binding to the Kinesin-2 tails, and such an interaction is critical for ciliary growth.

Kinesin-2 is required for the olfactory cilia growth and tubulin entry into the olfactory cilia in *Drosophila* antenna

Previous reports showed that the heterotrimeric kinesin-2 is sufficient for the assembly of all types of sensory cilia in *Drosophila* [4] and Zebrafish [14]. The ciliary outer segments are marked by Tubulin84B, which is homologous to α-tubulin1A/C. In addition, we found that the human orthologue, mRFP-αTub1A [52], localized at the outer segments of all sensory cilia, including the cilia inside *sensilla basiconica* (basiconic cilia) (Figure 6A), when expressed using the *chaGal4*. Therefore, we quantified the entry of RFP-αTub1A into the basiconic cilia in wild-type and homozygous $Klp64D^{k1}$ mutant backgrounds. In the latter case, the cilia appeared comparatively smaller, and there was an unusual accumulation of mRFP-Tub1A in the cell body (arrow, Figure 6A). Estimation of the ciliary growth, volume, and total mRFP intensity revealed that both the mRFP-Tub1A entry and ciliary growth was blocked in the mutant background (Figure 6B and C). Thus, it further suggested that heterotrimeric kinesin-2 is necessary for the cilia growth and tubulin entry into the cilia, which is consistent with the previous report [4].

Further, to test the role of kinesin-2 in tubulin transport inside the cilia, we measured the Fluorescent Recovery After Photobleach (FRAP) profiles of mRFP-Tub1A in the outer segment of the adult basiconic cilia (Figure 6D). We achieved a maximum recovery of 16.9% (±3.9) for mRFP-Tub1A and 39.1% (±4.2) for KLP64D-GFP after 500 seconds. A comparison of mRFP-Tub1A recovery at 250 seconds indicated significant reduction (9.4% ±2.4) in the mutant background, whereas the GFP recovery reached ~90% within 150 seconds in both wild-type and mutant backgrounds. The mRFP-Tub1A recovery was comparable to the maximum recovery of tubulin found in *C. elegans* before [18]. However, a scrutiny of the FRAP kymographs, collected at higher frame rates, revealed that neither the KLP64D-GFP nor the mRFP-Tub1A moved in a particulate form inside the ciliary outer segment. Hence, the data further suggested that the tubulin could be transported inside the cilia outer segment in dissociated form requiring kinesin-2.

Discussion:

IFT and the Bardet Biedl Syndrome complex are the major carriers of cargo into cilia/flagella assembly [53]. Genetic studies in *C. elegans* showed that particular

tubulin isoforms could be transported by two different types of kinesin-2 motors as part of the IFT in the sensory cilia [18]. A separate report also suggested that tubulin binds to the IFT74 and IFT81 heterodimer in vitro [19]. These data provided a generalized molecular mechanism of tubulin transport into the cilia and flagella. In this context, it would be important to note that direct observation in *Chlamydomonas* flagella using total internal reflection fluorescence microscopy indicated the existence of both IFT-dependent and diffusive forms of tubulin transport inside flagella [16]. In all these studies, the particulate form of tubulin movement inside the cilia is considered as the definitive indicator of IFT-mediated transport.

The outer segment of basiconic cilia grows in two distinct phases during pupal development [4]. Consistent with the previous observation we found that a mutation in the *Klp64D* locus significantly affects the tubulin entry and growth during the second phase. The tubulin recovery partly depended on the KLP64D, which is an essential component of the heterotrimeric kinesin-2. FRAP kymographs indicate that both Kinesin-2 and tubulin are transported in the ciliary outer segment in a non-particulate form. A similar recovery pattern was observed for the choline acetyltransferase in axon [28]. The latter directly binds to the C-terminal tails of the Kinesin-2α subunit. The non-particulate recovery suggests that tubulin could be transported in dissociated form, independent of IFT, in the basiconic cilia. Similarly, Kinesin-2 appeared to play an active role in managing this mode of transport inside sensory cilia. Altogether, these observations suggest that tubulin entry into the cilia could be assisted by a direct interaction between dissociated tubulin and kinesin-2 during the second growth phase.

Recent studies suggested several IFT and BBSome independent movements of cytoplasmic Dynein into the cilia [50]. Direct observations also revealed an IFT-independent movement of tubulin [17] and EB1 [54] inside *Chlamydomonas* flagella. Similarly, the ciliary entry of Phospholipase D (PLD), an AMP-dependent protein kinase, does not require the IFT and BBSome [55]. A diffusion-based model was suggested to facilitate the entry and propagation of these proteins into the cilia and along the axoneme. On the other hand, direct interactions between the Kif17 tail and Cyclic Nucleotide-Gated Channel B1b [51], as well as between KAP3 and Gli [27], are suggested to move them into primary cilia. Relatively little is known about the IFT-independent transport inside the bipartite axoneme-bearing sensory cilia. The results described here suggests the possibility of an IFT-independent entry of tubulin into the olfactory cilia in *Drosophila*.

The interaction between the tail domain and tubulin is also documented for many other kinesin-family motors through direct or indirect binding to tubulin or microtubule filaments [18, 19, 30, 31, 44, 56]. The interactions with the C-terminal tail domains of kinesin-1 [30] and the N-terminal tail domain of kinesin-14 [31] promotes microtubule stability [20, 30], which is indicated to help microtubule gliding in vivo. Kinesin-1 also binds to tubulin dimer through an adapter, CRMP-2, to transport them into the axon [56]. It would of interest to probe whether such interactions are isoform-specific. We found that the kinesin-2 tails bind to α-tubulin1 and the association does not increase microtubule stability. The dominant-negative disruption of cilia due to the tail overexpression in NIH3T3 cells, and its rescue by tubulin coexpression, further suggest that kinesin-2 tails could bind to dissociated tubulin which may compete with other essential, cilia-specific cargoes. It also highlights the relevance of this interaction in a cellular context. Hence, we suggest that such an interaction could facilitate the entry of specific tubulin isoforms into the cilia.

The cytoplasmic tubulin is purified as a stable dimer of two different (α, β) subunits. Each subunit has several different isoforms [57]. Often, the microtubule in various subcellular segments and tissues are found to contain a distinct set of α and β isotypes [7, 58-60]. Isotype composition can also define the properties of microtubule dynamics and tissue function [61, 62]. Although the axoneme is made of distinct α and β-tubulin isotypes [5-7, 60], a key question regarding the isotype selectivity remained unanswered. Our results suggest that Kinesin-2 tails could selectively bind to α-tubulin1A/D in dissociated form, which could enhance the isotype selectivity in combination with the IFT74/81 complex. It was intriguing that we failed to detect specific β isotypes

enrichment in the tail-pull down fraction of brain microtubule. It may suggest that other factors and specific local environment could further contribute to isoform-selective tubulin transport into the cilia and flagella.

Materials and methods:

The essential elements are provided below. A detailed description is provided in the supplemental methods.

DNA constructs

The Pm-sYFPC1 (super YFP), PmTQC1 (mTurquoise) plasmids were provided by J Goedhart [63]. PCR amplified tail specific DNA fragments of KLP64D and KLP68D tail sequences were inserted in the Pm-sYFPC1 between Bgl-II/Kpn-I sites; creating N-terminal sYFP fusion constructs of the tail fragments. Both the plasmids were sequenced, and expression was confirmed by immunostaining the cell lysate of transiently transfected cells for anti-GFP on western blots. For the bacterial expression, the sYFP-Tail sequence was PCR amplified from CMV vector and inserted in pETDuet™ vector using Hind III/Kpn I sites. K Verhey provided the Arl13b-mcherry containing plasmid with the consent from Kenji Kotani. The αTub84B cDNA was PCR amplified from *Drosophila melanogaster* total mRNA (1 µg); extracted using the Trizol method, oligo-dT primers, and Superscript III First-Strand Synthesis Kit; using 5'-CCGCGAATTCGGTACTCCTCAGCGCCCTC-3' (forward) and 5'-CCGCAGATCTATGAGAGAATGTATCTCTATC-3' (reverse) primers; and inserted into the Bgl-II/EcoR-I sites of Pm-TQC1. TQ–6aa-sYFP construct was prepared by attaching TQ and sYFP with the following intervening sequence 5'-CTGCAGGTCGACAAGCTT-3'. All other constructs were reported earlier [22, 28]. All recombinant proteins expressed in bacteria were purified according to established methods described before [28].

Drosophila heads and mouse brain extracts

Prepared using the standard protocol described in the supplemental methods. 100,000 xg supernatant was used for the blot overlay, affinity coprification, and cosedimentation assays.

Microtubule decoration on coverslips

Microtubules (MT) fixed on poly-lysine coated glass slides were incubated with 100 µl of equimolar (~0.02 µM) GST-KLP64DT or –KLP68DT solutions for 15 min. The slides were then immunostained using a standard protocol. For antibody competition, the slides were either incubated with 1/10 dilution of monoclonal supernatant or 0.01 µg/ml antibody solution; washed three times with PBS, and then incubated with the Kinesin-2 tail fragments.

Image acquisition and analysis

Zeiss CLSM 510 was used for image acquisition. All images were acquired using X63, NA 1.4 oil immersion objective. Ciliated cells were counted against total number of cells in each image field. For sFRET experiments, the cells were excited at 405 nm and imaged at 470-500 nm for TQ (donor fluorophore) and 530-600 nm for sYFP emissions. The acceptors (sYFP) was independently excited at 514 nm and imaged at 530-600 nm. To FRET values were calculated using the sYFP (acceptor) emission at 530-600 nm upon TQ (donor) excitation at 405 nm using the Metamorph™ software as described previously [47]. The following formula was used for calculating sFRET: $FRET_{corrected} = FRET_{raw} – A * sYFP – B * TQ$; A - fraction of sYFP excitation cross-talk in the FRET image (Calculated value 0.294); B - fraction of TQ emission cross-talk in the FRET channel (Calculated value 0.0208). Approximately, 10 to 15 cells were assessed for each set.

Morphological analysis of Drosophila olfactory cilia

All fly stocks used in this study, the pupal staging procedure and the morphological analysis technique were described before [4]. The olfactory cilia inside the LB-type *s. basiconica* shafts in an isolated antenna were imaged using X63 NA 1.35 oil immersion objective fitted on an Olympus FV1000SPD. The ciliary volume and total fluorescence intensity were estimated using ImageJ®. For the FRAP assay, the distal part (10 µm) of basiconic cilia was photobleached upto 60% below the initial intensity using appropriate laser power for 3 seconds, and then, imaged using 45-60 µW excitation power at either 0.2 (512x512 pixels) or 6 (100x45 pixels) frames per second (fps). The pixel dwell time was maintained at less than 4 µsec to minimize bleaching. Fluorescence recovery was quantified as %recovery of intensity as the following:

$$\% \text{ Fluorescence Recovery} = (Fr – Fa) \times 100/(Fb - Fa)$$

Fb and Fa indicate intensities before and after photobleaching while Fr is the fluorescence intensity recovered at time t. The sum of intensities of all pixels in the ROI was used for calculations.

Acknowledgments

We sincerely thank Balaji C and Hema Bagul of DBS, TIFR, for their help with LC-ESI-MS/MS experiment and analysis; Salitha Sashi for cloning; R Mallik, TIFR, India, as well as N Olieric and M Steinmetz, PSI, Switzerland, for various help. The project is funded by an intramural grant of TIFR, DAE, Govt. of India to KR, DP was funded by DAE-SRC fellowship and AK through a UGC fellowship.

Authors declare no conflict of interest with publishing the data.

References

1. Singla V, Reiter JF. The primary cilium as the cell's antenna: signaling at a sensory organelle. Science 2006;313:629-633.
2. Fisch C, Dupuis-Williams P. Ultrastructure of cilia and flagella - back to the future! Biol Cell 2011;103:249-270.
3. Silverman MA, Leroux MR. Intraflagellar transport and the generation of dynamic, structurally and functionally diverse cilia. Trends Cell Biol 2009;19:306-316.
4. Jana SC, Girotra M, Ray K. Heterotrimeric kinesin-II is necessary and sufficient to promote different stepwise assembly of morphologically distinct bipartite cilia in Drosophila antenna. Mol Biol Cell 2011;22:769-781.
5. Perkins LA, Hedgecock EM, Thomson JN, Culotti JG. Mutant sensory cilia in the nematode Caenorhabditis elegans. Dev Biol 1986;117:456-487.
6. Witman GB, Carlson K, Rosenbaum JL. Chlamydomonas flagella. II. The distribution of tubulins 1 and 2 in the outer doublet microtubules. J Cell Biol 1972;54:540-555.
7. Hurd DD, Miller RM, Nunez L, Portman DS. Specific alpha- and beta-tubulin isotypes optimize the functions of sensory Cilia in Caenorhabditis elegans. Genetics 2010;185:883-896.
8. Sharma N, Kosan ZA, Stallworth JE, Berbari NF, Yoder BK. Soluble levels of cytosolic tubulin regulate ciliary length control. Mol Biol Cell 2011;22:806-816.
9. Scholey JM. Kinesin-2: a family of heterotrimeric and homodimeric motors with diverse intracellular transport functions. Annual review of cell and developmental biology 2013;29:443-469.
10. Verhey KJ, Dishinger J, Kee HL. Kinesin motors and primary cilia. Biochem Soc Trans 2011;39:1120-1125.
11. Qin H, Diener DR, Geimer S, Cole DG, Rosenbaum JL. Intraflagellar transport (IFT) cargo: IFT transports flagellar precursors to the tip and turnover products to the cell body. J Cell Biol 2004;164:255-266.
12. Pedersen LB, Rosenbaum JL. Intraflagellar transport (IFT) role in ciliary assembly, resorption and signalling. Curr Top Dev Biol 2008;85:23-61.
13. Snow JJ, Ou G, Gunnarson AL, Walker MR, Zhou HM, Brust-Mascher I, Scholey JM. Two anterograde intraflagellar transport motors cooperate to build sensory cilia on C. elegans neurons. Nat Cell Biol 2004;6:1109-1113.
14. Zhao C, Omori Y, Brodowska K, Kovach P, Malicki J. Kinesin-2 family in vertebrate ciliogenesis. Proc Natl Acad Sci U S A 2012;109:2388-2393.
15. Pazour GJ, Dickert BL, Vucica Y, Seeley ES, Rosenbaum JL, Witman GB, Cole DG. Chlamydomonas IFT88 and its mouse homologue, polycystic kidney disease gene tg737, are required for assembly of cilia and flagella. J Cell Biol 2000;151:709-718.
16. Kozminski KG, Beech PL, Rosenbaum JL. The Chlamydomonas kinesin-like protein FLA10 is involved in motility associated with the flagellar membrane. J Cell Biol 1995;131:1517-1527.
17. Craft JM, Harris JA, Hyman S, Kner P, Lechtreck KF. Tubulin transport by IFT is upregulated during ciliary growth by a cilium-autonomous mechanism. J Cell Biol 2015;208:223-237.
18. Hao L, Thein M, Brust-Mascher I, Civelekoglu-Scholey G, Lu Y, Acar S, Prevo B, Shaham S, Scholey JM. Intraflagellar transport delivers tubulin isotypes to sensory cilium middle and distal segments. Nat Cell Biol 2011;13(7):790-798.
19. Bhogaraju S, Cajanek L, Fort C, Blisnick T, Weber K, Taschner M, Mizuno N, Lamla S, Bastin P, Nigg EA, Lorentzen E. Molecular basis of tubulin transport within the cilium by IFT74 and IFT81. Science 2013;341:1009-1012.
20. Karabay A, Walker RA. The Ncd tail domain promotes microtubule assembly and stability. Biochem Biophys Res Commun 1999;258:39-43.
21. Seeger M, Rice S. The Kinesin-1 Tail Binds to Microtubules in a Manner Similar to Tau. Biophys J 2010;98:370a-370a.
22. Doodhi H, Ghosal D, Krishnamurthy M, Jana SC, Shamala D, Bhaduri A, Sowdhamini R, Ray K. KAP, the accessory subunit of kinesin-2, binds the predicted coiled-coil stalk of the motor subunits. Biochemistry 2009;48:2248-2260.
23. Deacon SW, Serpinskaya AS, Vaughan PS, Lopez Fanarraga M, Vernos I, Vaughan KT, Gelfand VI. Dynactin is required for bidirectional organelle transport. J Cell Biol 2003;160:297-301.
24. Jimbo T, Kawasaki Y, Koyama R, Sato R, Takada S, Haraguchi K, Akiyama T. Identification of a link between the tumour suppressor APC and the kinesin superfamily. Nat Cell Biol 2002;4:323-327.
25. Mans DA, Lolkema MP, van Beest M, Daenen LG, Voest EE, Giles RH. Mobility of the von Hippel-Lindau tumour suppressor protein is regulated by kinesin-2. Experimental cell research 2008;314:1229-1236.
26. Baker SA, Freeman K, Luby-Phelps K, Pazour GJ, Besharse JC. IFT20 links kinesin II with a mammalian intraflagellar transport complex that is conserved in motile flagella and sensory cilia. J Biol Chem 2003;278(36):34211-34218.
27. Carpenter BS, Barry RL, Verhey KJ, Allen BL. The heterotrimeric kinesin-2 complex interacts with and

regulates GLI protein function. J Cell Sci 2015;128:1034-1050.
28. Sadananda A, Hamid R, Doodhi H, Ghosal D, Girotra M, Jana SC, Ray K. Interaction with a kinesin-2 tail propels choline acetyltransferase flow towards synapse. Traffic 2012;13:979-991.
29. Fan J, Beck KA. A role for the spectrin superfamily member Syne-1 and kinesin II in cytokinesis. J Cell Sci 2004;117:619-629.
30. Seeger MA, Rice SE. Microtubule-associated protein-like binding of the kinesin-1 tail to microtubules. J Biol Chem 2010;285:8155-8162.
31. Karabay A, Walker RA. Identification of microtubule binding sites in the Ncd tail domain. Biochemistry 1999;38:1838-1849.
32. Karabay A, Walker RA. Identification of Ncd tail domain-binding sites on the tubulin dimer. Biochem Biophys Res Commun 2003;305:523-528.
33. Saoudi Y, Paintrand I, Multigner L, Job D. Stabilization and bundling of subtilisin-treated microtubules induced by microtubule associated proteins. J Cell Sci 1995;108:357-367.
34. Wendt T, Karabay A, Krebs A, Gross H, Walker R, Hoenger A. A structural analysis of the interaction between ncd tail and tubulin protofilaments. J Mol Biol 2003;333:541-552.
35. Stauber T, Simpson JC, Pepperkok R, Vernos I. A role for kinesin-2 in COPI-dependent recycling between the ER and the Golgi complex. Curr Biol 2006;16:2245-2251.
36. Navone F, Niclas J, Hom-Booher N, Sparks L, Bernstein HD, McCaffrey G, Vale RD. Cloning and expression of a human kinesin heavy chain gene: interaction of the COOH-terminal domain with cytoplasmic microtubules in transfected CV-1 cells. J Cell Biol 1992;117:1263-1275.
37. Hollenbeck PJ. The distribution, abundance and subcellular localization of kinesin. J Cell Biol 1989;108:2335-2342.
38. Cai D, Verhey KJ, Meyhofer E. Tracking single Kinesin molecules in the cytoplasm of mammalian cells. Biophys J 2007;92:4137-4144.
39. Janke C, Kneussel M. Tubulin post-translational modifications: encoding functions on the neuronal microtubule cytoskeleton. Trends Neurosci 2010;33(8):362-372.
40. Song Y, Kirkpatrick LL, Schilling AB, Helseth DL, Chabot N, Keillor JW, Johnson GV, Brady ST. Transglutaminase and polyamination of tubulin: posttranslational modification for stabilizing axonal microtubules. Neuron 2013;78:109-123.
41. Edde B, Rossier J, Le Caer JP, Desbruyeres E, Gros F, Denoulet P. Posttranslational glutamylation of alpha-tubulin. Science 1990;247:83-85.
42. Redeker V, Rusconi F, Mary J, Prome D, Rossier J. Structure of the C-terminal tail of alpha-tubulin: increase of heterogeneity from newborn to adult. Journal of neurochemistry 1996;67:2104-2114.
43. Ait-Belkacem R, Calligaris D, Sellami L, Villard C, Granjeaud S, Schembri T, Berenguer C, Ouafik L, Figarella-Branger D, Chinot O, Lafitte D. Tubulin isoforms identified in the brain by MALDI in-source decay. Journal of proteomics 2013;79:172-179.
44. Seidel C, Zekert N, Fischer R. The Aspergillus nidulans Kinesin-3 Tail Is Necessary and Sufficient to Recognize Modified Microtubules. Plos One 2012;7(2).
45. Cai D, Hoppe AD, Swanson JA, Verhey KJ. Kinesin-1 structural organization and conformational changes revealed by FRET stoichiometry in live cells. J Cell Biol 2007;176:51-63.
46. Avidor-Reiss T, Maer AM, Koundakjian E, Polyanovsky A, Keil T, Subramaniam S, Zuker CS. Decoding cilia function: defining specialized genes required for compartmentalized cilia biogenesis. Cell 2004;117:527-539.
47. Broussard JA, Rappaz B, Webb DJ, Brown CM. Fluorescence resonance energy transfer microscopy as demonstrated by measuring the activation of the serine/threonine kinase Akt. Nature protocols 2013;8:265-281.
48. Li Y, Ling K, Hu J. The emerging role of Arf/Arl small GTPases in cilia and ciliopathies. J Cell Biochem 2012;113(7):2201-2207.
49. Leaf A, Von Zastrow M. Dopamine receptors reveal an essential role of IFT-B, KIF17, and Rab23 in delivering specific receptors to primary cilia. Elife 2015;4.
50. Hao L, Efimenko E, Swoboda P, Scholey JM. The retrograde IFT machinery of C. elegans cilia: two IFT dynein complexes? Plos One 2011;6:e20995.
51. Jenkins PM, Hurd TW, Zhang L, McEwen DP, Brown RL, Margolis B, Verhey KJ, Martens JR. Ciliary targeting of olfactory CNG channels requires the CNGB1b subunit and the kinesin-2 motor protein, KIF17. Curr Biol 2006;16:1211-1216.
52. Rusan NM, Peifer M. A role for a novel centrosome cycle in asymmetric cell division. J Cell Biol 2007;177:13-20.
53. Bhogaraju S, Engel BD, Lorentzen E. Intraflagellar transport complex structure and cargo interactions. Cilia 2013;2:10.
54. Harris JA, Liu Y, Yang P, Kner P, Lechtreck KF. Single-particle imaging reveals intraflagellar transport-independent transport and accumulation of EB1 in Chlamydomonas flagella. Mol Biol Cell 2016;27:295-307.
55. Lechtreck KF, Brown JM, Sampaio JL, Craft JM, Shevchenko A, Evans JE, Witman GB. Cycling of the signaling protein phospholipase D through cilia requires

the BBSome only for the export phase. J Cell Biol 2013;201:249-261.
56. Kimura T, Watanabe H, Iwamatsu A, Kaibuchi K. Tubulin and CRMP-2 complex is transported via Kinesin-1. Journal of neurochemistry 2005;93:1371-1382.
57. Lopata MA, Cleveland DW. In vivo microtubules are copolymers of available beta-tubulin isotypes: localization of each of six vertebrate beta-tubulin isotypes using polyclonal antibodies elicited by synthetic peptide antigens. J Cell Biol 1987;105:1707-1720.
58. Leandro-Garcia LJ, Leskela S, Landa I, Montero-Conde C, Lopez-Jimenez E, Leton R, Cascon A, Robledo M, Rodriguez-Antona C. Tumoral and tissue-specific expression of the major human beta-tubulin isotypes. Cytoskeleton (Hoboken) 2010;67:214-223.
59. Hoyle HD, Raff EC. Two Drosophila beta tubulin isoforms are not functionally equivalent. J Cell Biol 1990;111:1009-1026.
60. Savage C, Hamelin M, Culotti JG, Coulson A, Albertson DG, Chalfie M. mec-7 is a beta-tubulin gene required for the production of 15-protofilament microtubules in Caenorhabditis elegans. Genes Dev 1989;3:870-881.
61. Bhattacharya R, Yang H, Cabral F. Class V beta-tubulin alters dynamic instability and stimulates microtubule detachment from centrosomes. Mol Biol Cell 2011;22:1025-1034.
62. Hari M, Yang H, Zeng C, Canizales M, Cabral F. Expression of class III beta-tubulin reduces microtubule assembly and confers resistance to paclitaxel. Cell Motil Cytoskeleton 2003;56:45-56.
63. Goedhart J, van Weeren L, Hink MA, Vischer NOE, Jalink K, Gadella TWJ. Bright cyan fluorescent protein variants identified by fluorescence lifetime screening. Nat Methods 2010;7:137-U174.

Figure legends

Figure 1: Kinesin-2 tails bind to tubulin *in vitro*. A) Schematic illustrates heterotrimeric kinesin-2 composition and the tail sequences of the motor subunits KLP64D and KLP68D, respectively. **B)** Ni-NTA copurification of tubulin with heterotrimeric kinesin-2 complex from the head extract of *Drosophila* expressing KLP64D-Tev-His (bait) and either KLP68D-YFP or DmKAP-RFP. The head extracts of the background stocks expressing only KLP68D-YFP or DmKAP-RFP were used for Ni-NTA bead control. **C)** Blot overlay assays with the recombinant GST-tail fragments. Western blots of soluble fly head extract were separated on a 12% SDS-PAGE and overlaid with purified GST-KLP64DT **(a)** and GST-KLP68DT **(b)**, and immunostained with anti-GST **(a, b)** and anti-α-tubulin **(c)**. Arrow and arrowhead indicate prominent interacting bands in **(a)** and **(b)**, and the arrow indicates the α-tubulin band in **(c)**. **D)** Tubulin copurification with KLP64D and KLP68D tail fragments by affinity chromatography. **E, F)** Cosedimentation of KLP64DT and KLP68DT **(E)**, as well as the KIF3AT and KIF3BT **(F)** with purified goat brain microtubule in the presence of 20 μM Taxol. Average Kd for Kif3A tail and tubulin binding is 3.6+1.8 μM (n = 3). **G)** Ni-NTA copurification of tubulin in the presence of 20 μM colchicine (chl) from the head extracts of *Drosophila* expressing KLP64D-Tev-His or KLP64DΔT-Tev-His and KLP68DΔT-YFP, respectively.

Figure 2: C-terminal 'tail' domain of αTubulin is essential for binding to the recombinant kinesin-2 tails. A) Microtubule Filaments fixed on glass coverslips were decorated with either GST-KLP64DT or GST-KLP68DT fragments, and then immunostained with Anti-GST and Anti-αTubulin. **B)** A similar experiment performed with 0.01 μg/ml anti-αTubulin pretreatment before the recombinant kinesin-2 tail incubations. It eliminated the anti-GST staining of the microtubule filaments, indicating that the antibody binding blocked the interaction between kinesin-2 tail and tubulin. **C**) Purified Goat brain tubulin, treated with subtilisin in different combinations as shown on the panel, was separated in SDS-PAGE and stained using Coomassie blue. It revealed relative shifts in the β and α tubulin-specific bands after the treatments due to the loss of C-terminal 'tail' sequence. **D**) In vitro decoration of microtubule after the subtilisin treatments with 6xHis-sYFP-KLP64DT and 6xHis-sYFP-KLP68DT revealed that kinesin-2 tails interact with c-terminal residues of alpha-tubulin.

Figure 3: Kinesin-2 tails have a relatively higher affinity to tissue-specific tubulin isoforms. A) NIH3T3 cells, transfected with pCMV-sYFP-KLP64DT and pCMV-sYFP-KLP68DT, respectively, were grown for 48 hours and then immunostained with tubulin (red). Most of the recombinant tails localized in the ER. **B)** HeLa cells were separately loaded with 0.1μg/ml GST-KLP64DT and GST-KLP68DT, respectively, using glass bead loading technique, then fixed and immunostained with both the anti-α-tubulin (green) and anti-GST (red). The anti-GST staining is mostly localized in the ER and did not colocalize with microtubule in the cells. Scale bars indicate 10 μm for all the figures and Insets show enlarged views microtubules from a part of the cells. **C)** Affinity chromatography using purified GST-KLP64D and GST-KLP68D tail fragments with different mouse tissue extracts (**a**, abbreviations: B-Brain, SN- Sciatic Nerve, L-Liver, K-Kidney, M-Muscle). Glutathione Sepharose® bead eluates **(b, c)** were separated in SDS-PAGE, western-blotted and immunostained with anti-α-tubulin and anti-GST antibodies. **D)** Sedimentation in the

presence of increasing molar concentrations of GST-KLP64DT **(a)** and GST-KLP68DT **(b)** as indicated by the tail:tubulin ratio on the top row. The pellet (p) and supernatant (s) fractions were separated in SDS-PAGE and stained with Coomassie blue. A similar experiment was performed in the presence of different concentrations of taxol **(c)** demonstrated a visible increase in the tubulin yield in the pellet fractions with increasing concentrations. **E)** A similar experiment performed using recombinant GST-KIF3AT (a), GST–KIF3BT (b), and GST (c), respectively, and the pellet fractions were estimated by SDS-PAGE.

Figure 4: Kinesin-2 tails pulled down α-tubulin1A/D isoforms from the goat brain preparations. A) SDS-PAGE separation of tubulin co-purified with recombinant (GST) Kinesin-2 tails. **B)** LC profiles of the isolated gel bands. In 8 out of 12 occasions, the ESI-MS/MS identified tubulinA1 isoforms with a maximum confidence score (Supplemental Table 2). **C)** NIH3T3 cells were co-transfected with pCMV-SYFP-KLP68DT and pCMV-TQ-Tubulin84B constructs. Forster's resonance energy transfer (FRET) efficiency between the TQ and sYFP, measured using sensitized emission technique, is shown on the right panel. **D)** Histograms depict integrated FRET efficiency (Average $\pm$ S.D., n>7, N = 3) between TQ-Tubulin84B and sYFP-KLP64DT, as well as sYFP-KLP68DT, and normalized for the bleed through, as well as the expression levels of both the fluorophores, according to the established protocol. A conjugated sYFP-6aa-TQ recombinant protein was used as positive control and co-expression of pCMV-sYFP and pCMV-TQ was used as negative control (*also see* Table S2).

Figure 5: Overexpression of kinesin-2 tails disrupts cilia growth in NIH3T3 cells. A) Recombinant sYFP, sYFP-KLP64DT, and sYFP-KLP68DT, respectively, were expressed in the NIH3T3 cells. Acetylated-α-Tubulin immunostaining highlighted the cilia (arrows). **B)** TQ-Tubulin84B and sYFP-KLP68DT were coexpressed in the NIH3T3 cells, and acetylated-α-Tubulin immunostaining marked the cilium (arrow). **C)** Histograms depict the average fraction of ciliated cells ($\pm$ S.D.) estimated by anti-acetylated-α-tubulin staining. A minimum of three cohorts containing 20-30 cells each was used for the estimate in each case. The pairwise significance of differences was calculated using Students' T-test and the p-values ('*' <0.1, '**' <0.01, and '***'<0.001) are indicated by the bars. **D)** The cilia expression profile in the Arl13b-mCherry coexpressed backgrounds. **E)** Histograms depict the distribution of cilia estimated in independently transfected cohorts by either Arl13b-mCherry coexpression or by anti-acetylated-α-tubulin staining. The set stained with anti-acetylated-α-tubulin was not cotransfected with Arl13b-mCherry. The data shown in C and E were acquired from separate batches.

Figure 6: Mutation in the *Klp64D* gene affects tubulin transport into the olfactory cilia in *Drosophila*. A) Recombinant mRFP-Tubulin1A localizations in the basiconic cilia (arrowheads) in wild-type (a) and homozygous *Klp64D*^{k1} (b) mutant backgrounds at 84h after pupa formation (APF). The arrow (b) indicates the accumulation of the recombinant tubulin the neuronal cell body and the scale bar marks 5 μm. **B)** The relative mRFP-Tub1A fluorescence and the ciliary volume estimates from individual basiconic cilia in wild-type (cyan) and homozygous *Klp64D*^{k1} (red) backgrounds were plotted against each other. It indicates that both the ciliary volume and the mRFP-Tubulin1A localization were reduced in the mutant. **C)** The table shows the number of cilia in different volume segments at three separate stages of pupal development (hours APF), in wild-type and homozygous *Klp64D*^{k1} mutant backgrounds. The cilia growth defect was rescued by transgenic expression of UAS-KLP64D-GFP in the *Klp64D*^{k1} background (4). **D)** Fluorescence Recovery After Photobleaching (FRAP) analysis of the GFP, KLP64D-GFP, and mRFP-Tubulin flow into the basiconic cilia in freshly eclosed adult *Drosophila* antennae. (a) The relative FRAP recovery profiles suggest that mRFP-Tubulin (red) turnover was slower as compared to that of the KLP64D-GFP (cyan), which was further reduced in the homozygous *Klp64D*^{k1} background (green) (Movies S1-4). (b) The kymographs generated from time-lapse acquisitions at 6 fps indicate the absence of IFT-like particulate movements of KLP64D-GFP and GFP-Tub84B in the cilia.

Supporting Information:

Supplemental data: Sequence homology and structure prediction analysis of kinesin-2 and Tubulin tails, and methods detail.

Figure S1: Kinesin-2 interacts with tubulin in the absence of ATP. A) Coimmunoprecipitation of tubulin with kinesin-2, and vice versa, from mouse brain homogenate. Anti-Kif3A (rabbit) pulled down mouse brain tubulin along with limited amount of KLC and not GAPDH, which is a known interactor of Kinesin-1. B) Blot overlay assays with the recombinant GST-tail fragments. Western blots of soluble mouse brain extracts separated on a 12% SDS-PAGE were overlaid with purified GST-KLP64DT and GST-KLP68DT, and immunostained with anti-GST and anti-α-tubulin. Arrows indicate prominent

interacting bands. C) GST-KIF3A cosedimented with 20 μM, taxol-stabilized, microtubule with an average affinity of 3.6+1.8 μM.

Figure S2: Kinesin-2 tail fragments colocalized with the endoplasmic reticulum (ER) in tissue cultured cells. NIH3T3 cells cotransfected with the pCMV-dsRED-KDEL (an ER label in live cells), and pCMV-sYFP-KLP68DT (A-A') or pCMV-sYFP-KLP64DT (B-B'), respectively. They were immunostained with the α-tubulin antibody.

Figure S3: Kiensin-2 tails pulled down dissociated tubulin dimer. Purified Goat brain tubulin was incubated in 100 mM phosphate-buffered saline (PBS) at room temperature for 2, 6 and 10 hours before affinity copurification with the GST-tagged kinesin-2 tail fragments. The bead eluates and flow-through fractions were probed with acetylated α-tubulin and β-tubulin antisera, respectively, after western blotting.

Figure S4: Kinesin-2 tails pull down all five β-tubulin isotypes from the goat brain preparation in similar proportion present in the input tissue. Immune analysis of β tubulin isoforms in the affinity pull-down content of the recombinant kinesin-2 tails. The bead extracts were separated by SDS-PAGE and analyzed using β tubulin specific antibodies as shown below.

Figure S5: Quantification of blots from figure 1.

Figure S6: Quantification of blots from figure 3.

Table S1: LC-ESI-MS/MS identification of tubulin copurified with the recombinant kinesin-2 tails.

Table S2: LC-ESI-MS/MS identification of tubulin isoforms in different sets of pull-down with Kinesin-2 tail fragments.

Table S3: Average Forster's Resonance Energy Transfer (FRET) efficiency (+ S.D.) between the various donor-acceptor pairs expressed in the NIH3T3 cells.

Table S4: LC-ESI-MS/MS analysis of Kinesin-2 tail fragments, generated by endopeptidase, and co-sedimented with microtubule after the protease digestion.

Movie S1: GFP FRAP in the adult basiconic cilia at 0.2 fps.

Movie S2: KLP64D-GFP FRAP in the adult basiconic cilia at 0.2 fps.

Movie S3: mRFP-Tub1A FRAP in the adult basiconic cilia at 0.2 fps.

Movie S4: mRFP-Tub1A FRAP in the adult basiconic cilia from homozygous *Klp64D*^{k1} at 0.2 fps

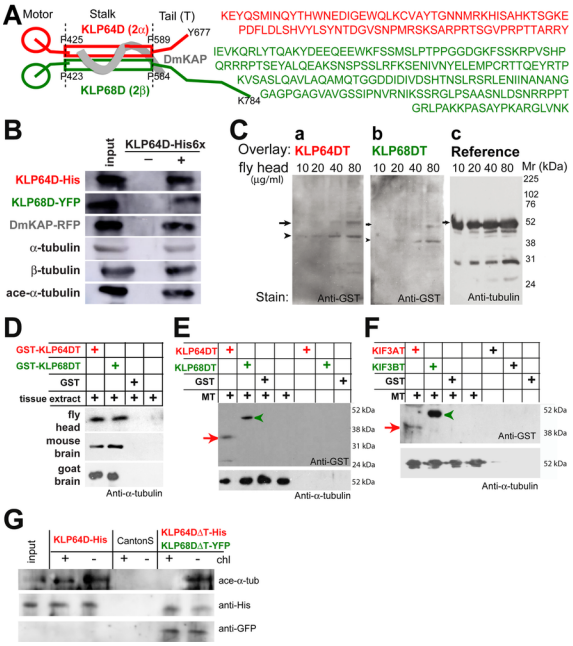

Figure 1 Girotra et al 2Dec2016.tif

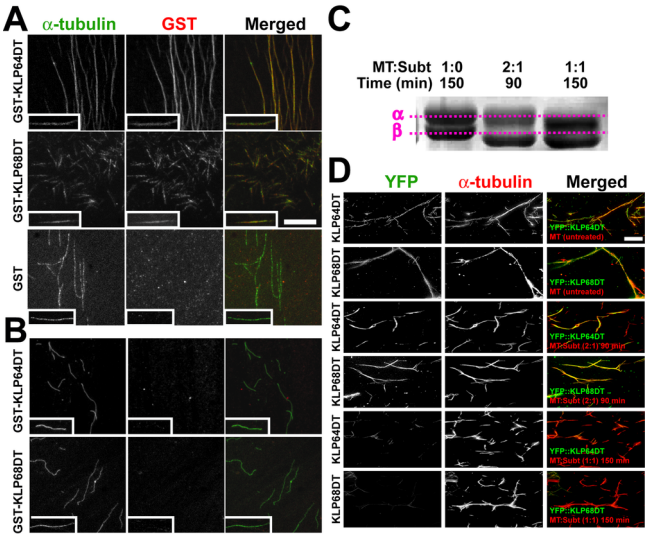

Figure 2 Girotra et al 11Nov2014a.tif

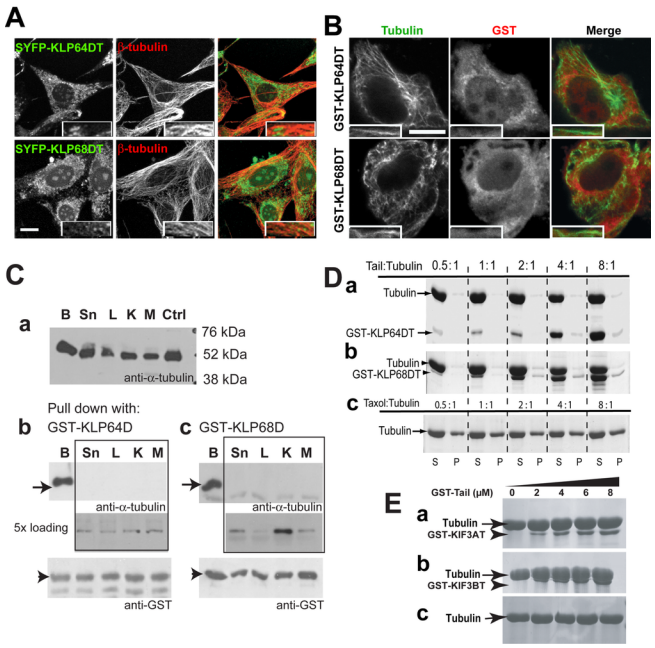

Figure 3 Girotra et al 30Nov2014.tif

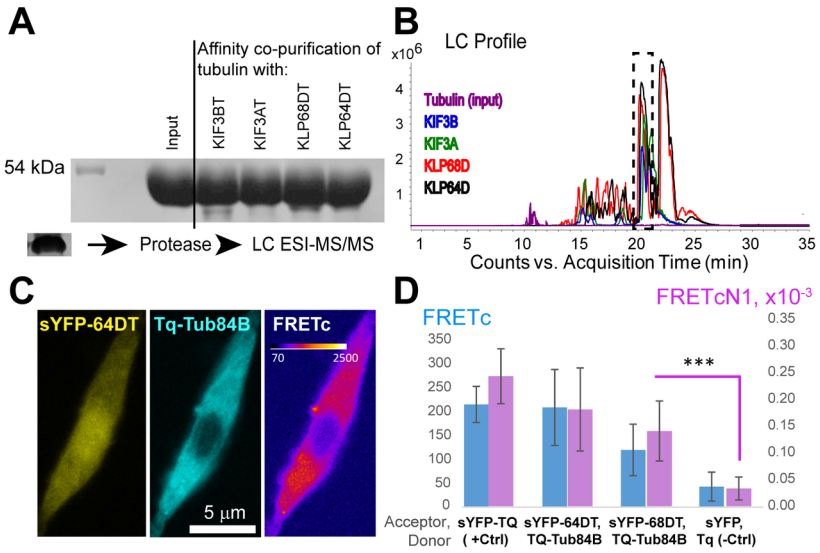

Figure 4 Girotra et al 20Marchl2016.tif

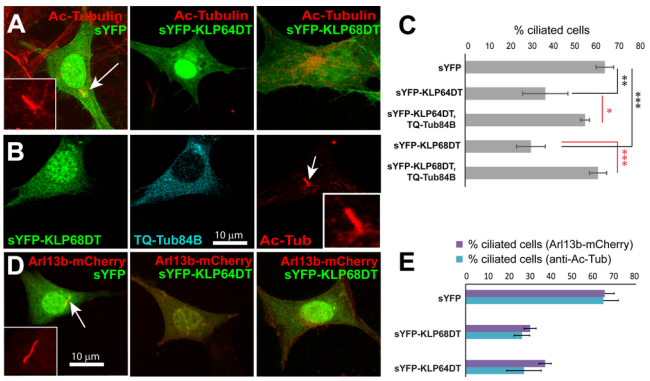

Figure 5 Girotra et al 4Dec2016.tif

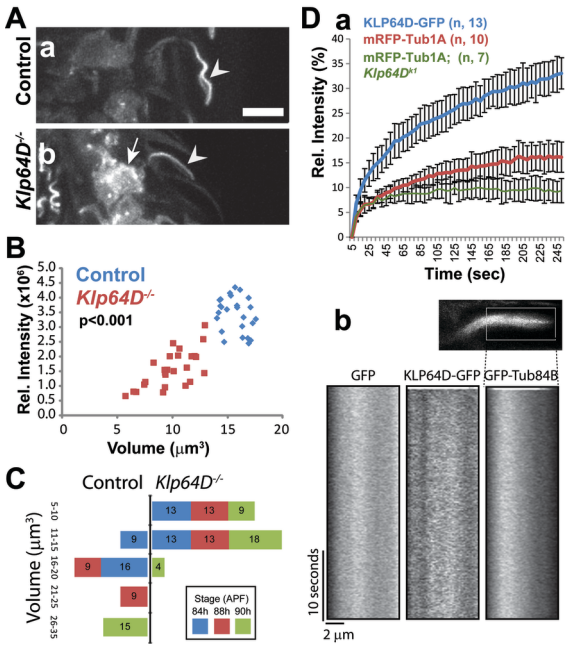

Figure 6 Girotra et al 24 April 2016.tif

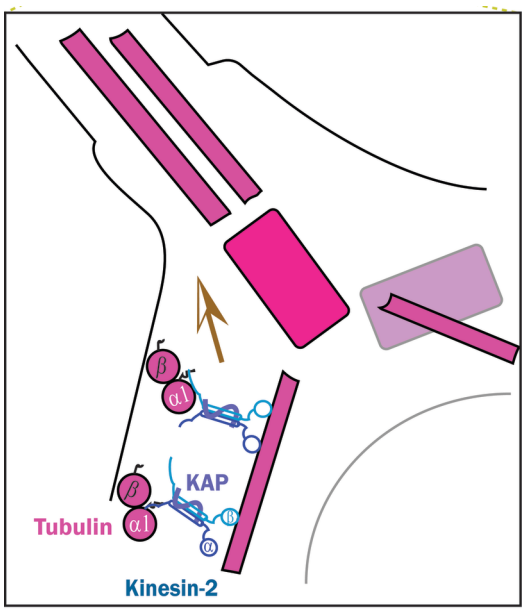

IFT-independent tublin transport into cilia

tra_12461_AbstractFigure.tif